Supplementary Information

of

Amorphous molybdenum sulfide nanocatalysts simultaneously realizing efficient upgrading of residue and synergistic synthesis of 2D MoS_2 nanosheets/carbon hierarchical structures

Yajing Duan,[a,b] Yanglin Liu,[c] Zhaojun Chen,[a] Dong Liu,*[d] Enqiang Yu,[e] Xiaodong Zhang,[a] Hui Fu,[a] Jinzhe Fu,[a] Jiatao Zhang*[f] and Hui Du*[a]

a. College of Chemistry and Chemical Engineering, Qingdao University, Qingdao, Shandong 266071, China

b. College of Physics, Qingdao University, Qingdao, Shandong 266071, China

c. School of Computer Science and Technology, BIT, Beijing Institute of Technology, Beijing, 100081, China

d. State Key Laboratory of Heavy Oil Processing, China University of Petroleum, Qingdao, Shandong 266580, China

e. China Offshore Bitumen Co., Ltd, China National Offshore Oil Corp, Binzhou, Shandong 256600, China

f. Beijing Key Laboratory of Construction-Tailorable Advanced Functional Materials and Green Applications, School of Materials Science & Engineering, Beijing Institute of Technology, Beijing 100081, China

***Corresponding Author**

Dong Liu: E-mail: liudong@upc.edu.cn. Tel.: +86-532-86980381

Jiatao Zhang: E-mail: zhangjt@bit.edu.cn. Tel.: +86-10-68918065

Hui Du: E-mail: duhui@qdu.edu.cn. Tel.: +86-532-85955529.

Table S1. Composition and properties of SZVR.

ρ^{20} ($g \cdot cm^{-1}$)	ν ($mm^2 \cdot s^{-1}$)	Carbon residue (wt %)	Elemental composition (wt %)			
			C	H	S	N
1.021	1258 (100 °C)	21.16	86.86	10.80	0.68	0.97
SARA (wt %)				Metal ($\mu g \cdot g^{-1}$)		
Saturates	Aromatics	Resin	*n*-C_7 asphaltene	Ni	V	Fe
21.29	29.81	36.38	12.52	18.9	1.65	15.8

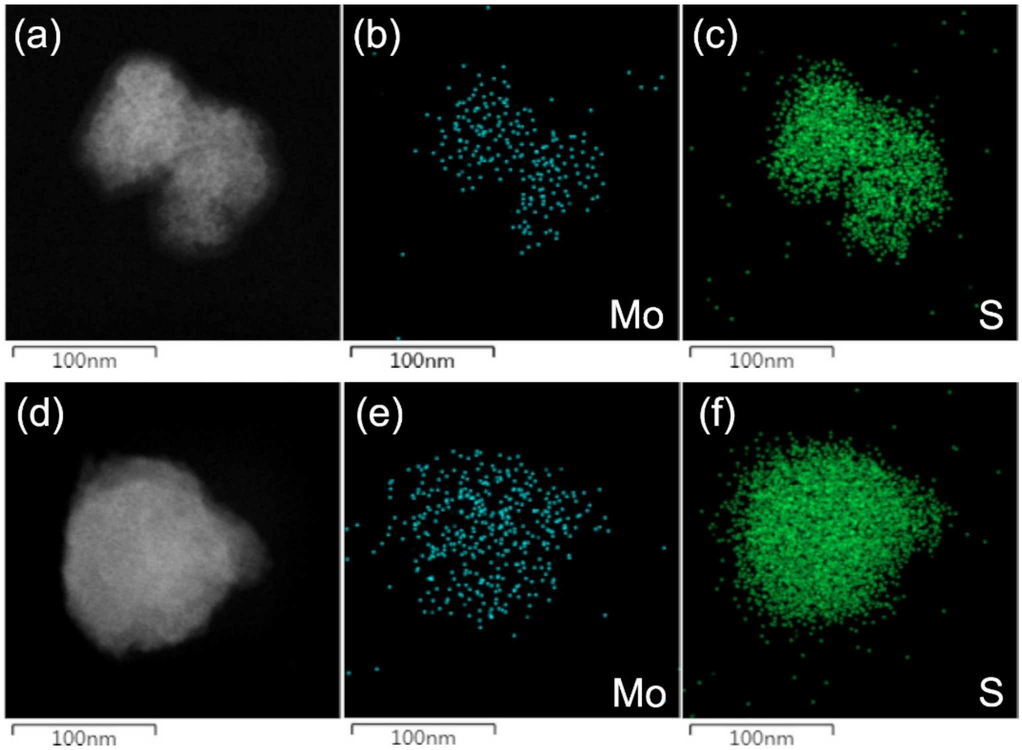

Figure S1. TEM image and the corresponding elemental mapping images of Mo, S of (a-c) MoSx-AM and (d-f) MoSx-OL.

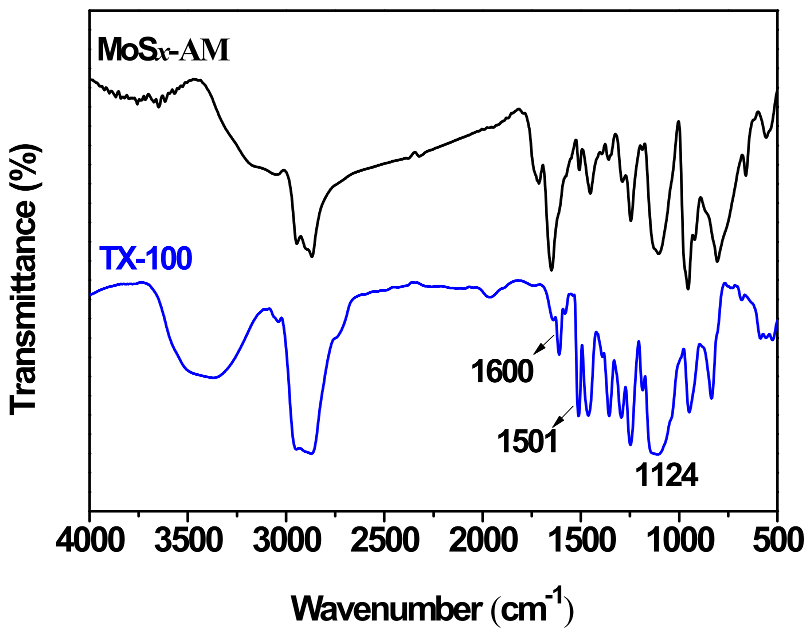

Figure S2. FTIR spectra of MoS*x*-AM and Triton X-100.

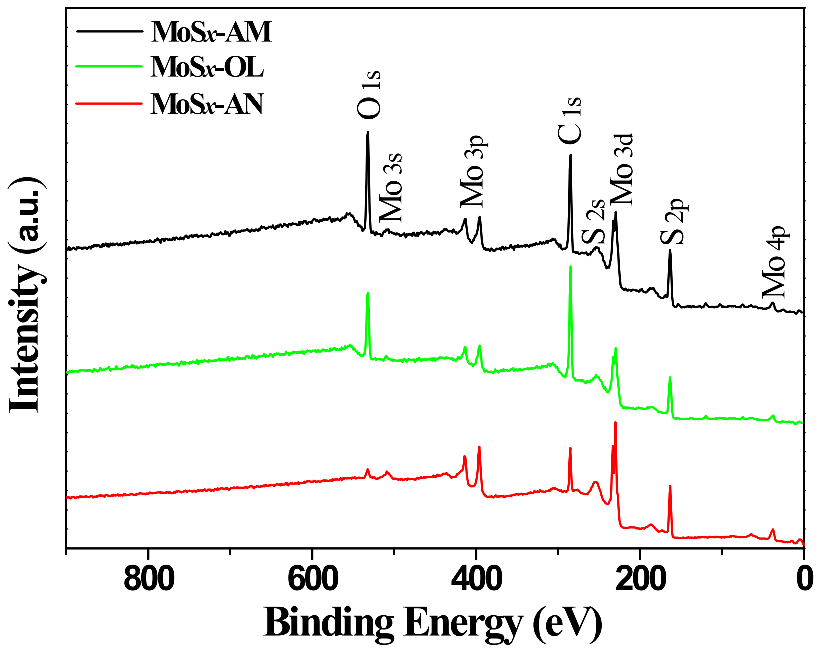

Figure S3. XPS survey spectra of MoS*x* nanocatalysts samples.

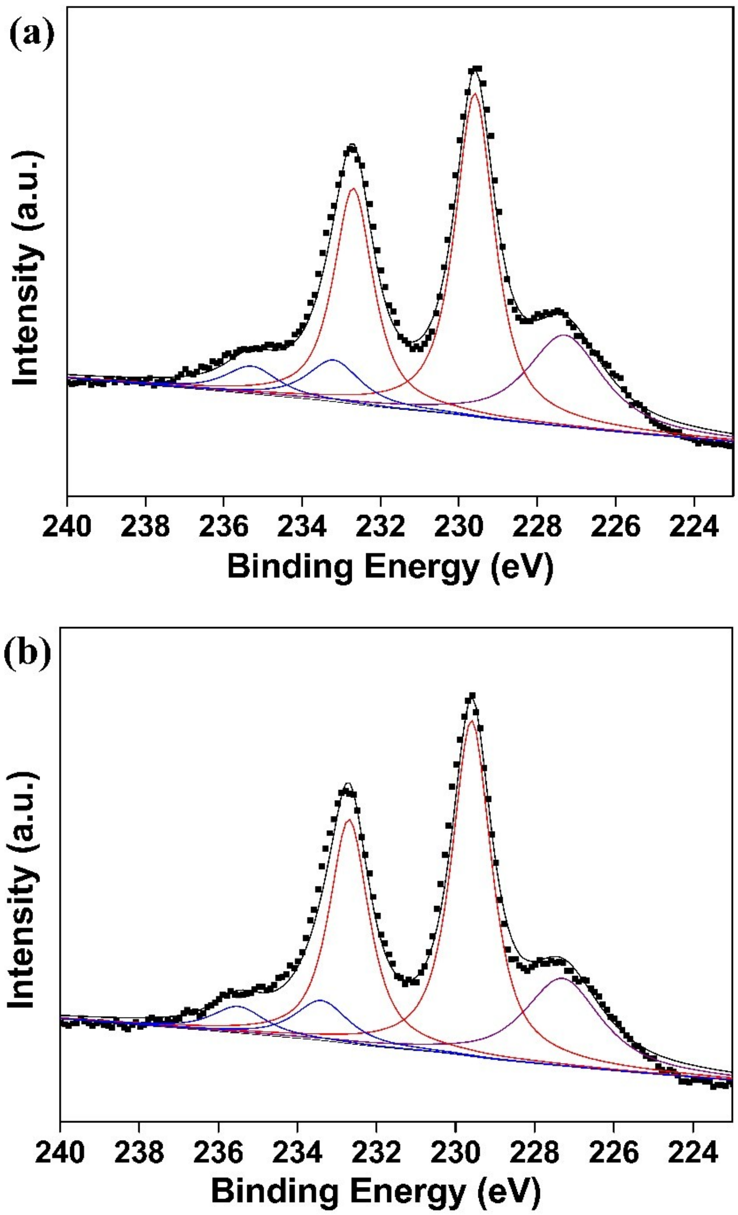

Figure S4. High-resolution Mo 3d spectra of (a) MoS*x*-AM and (b) MoS*x*-OL. (Dashed lines are raw data, black lines are fitted data, red lines are $3d_{5/2}$ and $3d_{3/2}$ orbital curves of Mo^{4+}, blue lines are $3d_{5/2}$ and $3d_{3/2}$ orbital curves of Mo^{6+}, purple lines are orbital curves of S 2s.)

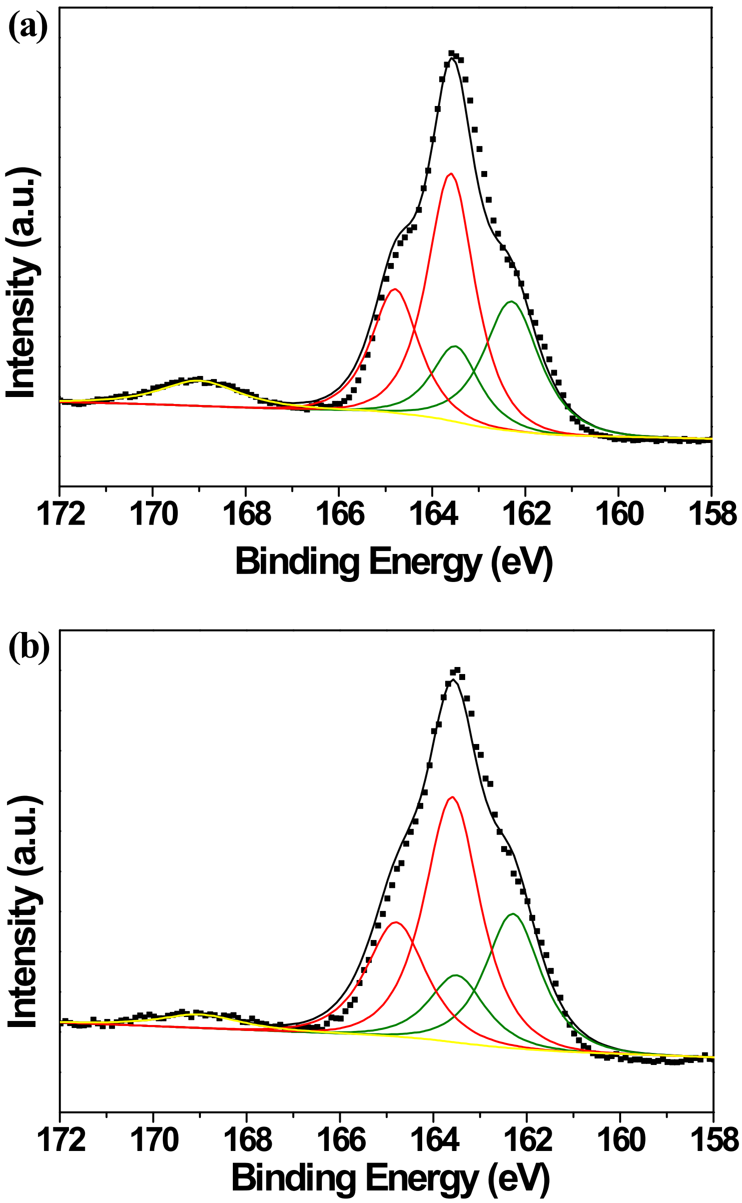

Figure S5. High-resolution S 2p spectra of (a) MoS*x*-AM and (b) MoS*x*-OL. (Dashed lines are raw data, black lines are fitted data, olive lines are S $2p_{3/2}$ and S $2p_{1/2}$ orbital curves of unsaturated S^{2-} and terminal S_2^{2-}, red lines are S $2p_{3/2}$ and S $2p_{1/2}$ orbital curves of apical S^{2-} and bridging S_2^{2-}, yellow lines are orbital curves of S^{6+}.)

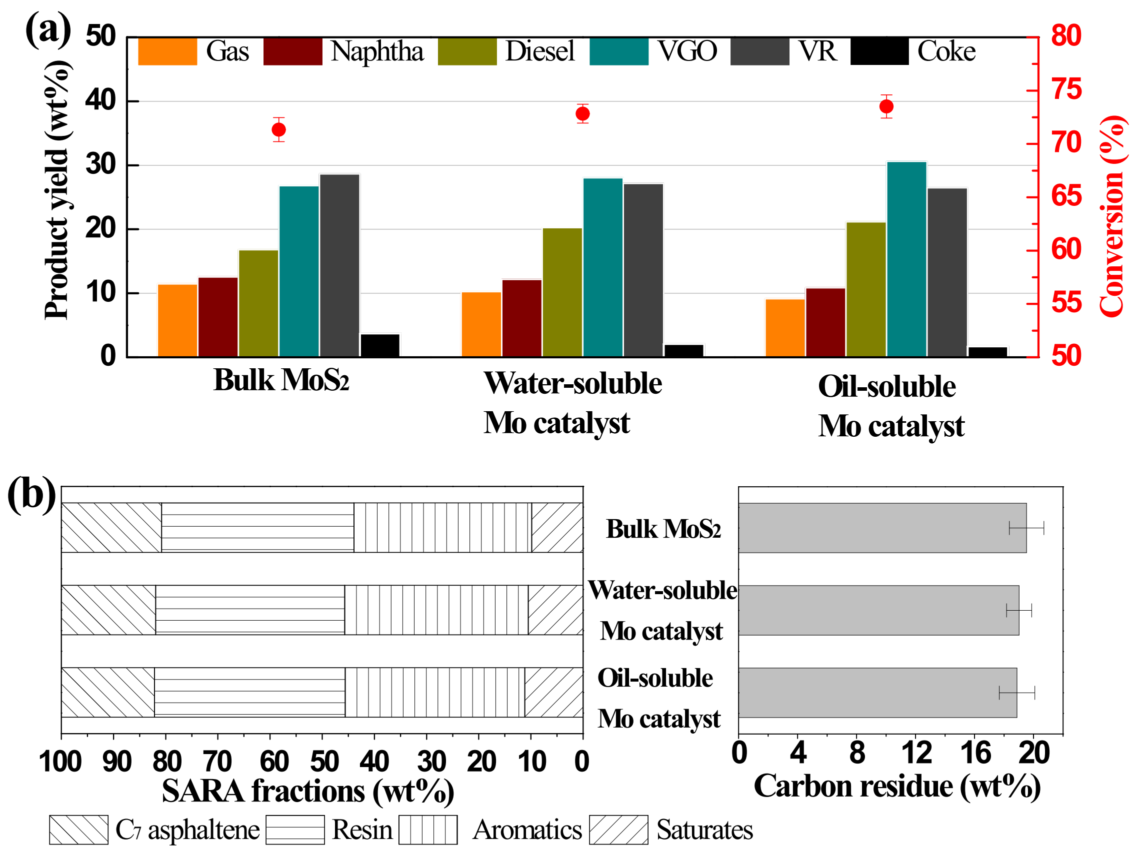

Figure S6. (a) Product distribution and conversion, and (b) SARA composition and Conradson carbon residue of VR products from SZVR slurry-phase hydrocracking with different Mo-based catalysts.

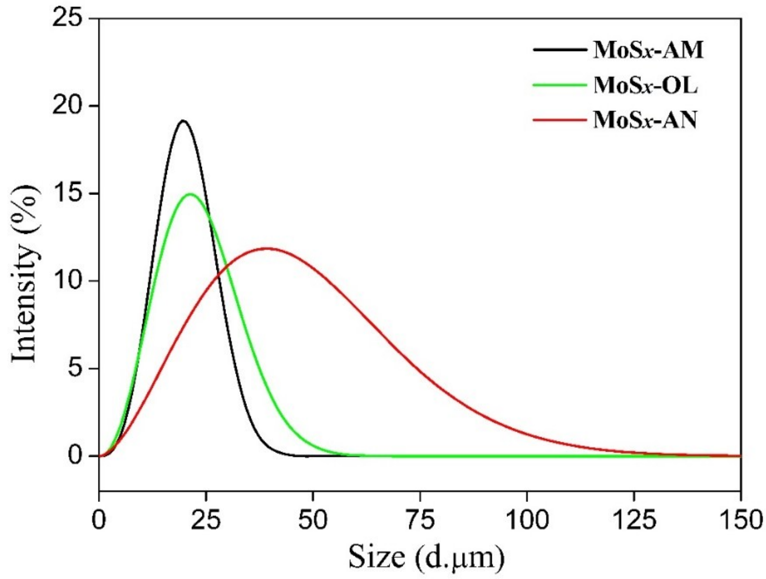

Figure S7. Size distribution of the coke products from SZVR slurry-phase hydrocracking with different MoSx nanocatalysts.

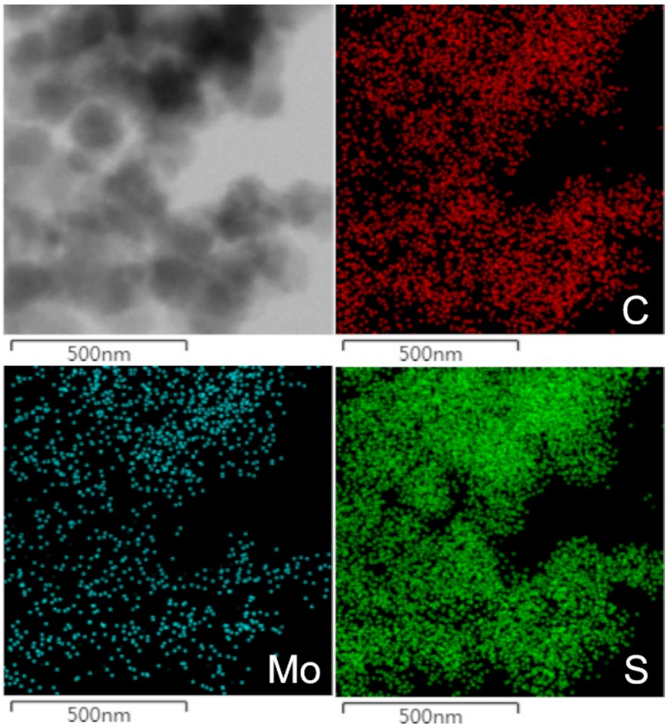

Figure S8. TEM image and the corresponding EDS elemental mapping images of C, Mo, S of the solid products from SZVR slurry-phase hydrocracking with MoS*x*-AM.

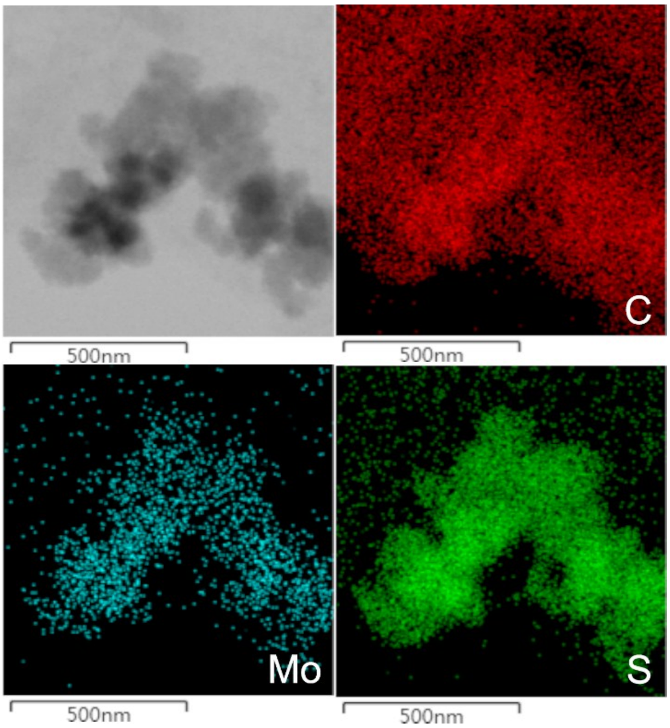

Figure S9. TEM image and the corresponding EDS elemental mapping images of C, Mo, S of the solid products from SZVR slurry-phase hydrocracking with MoS*x*-OL.

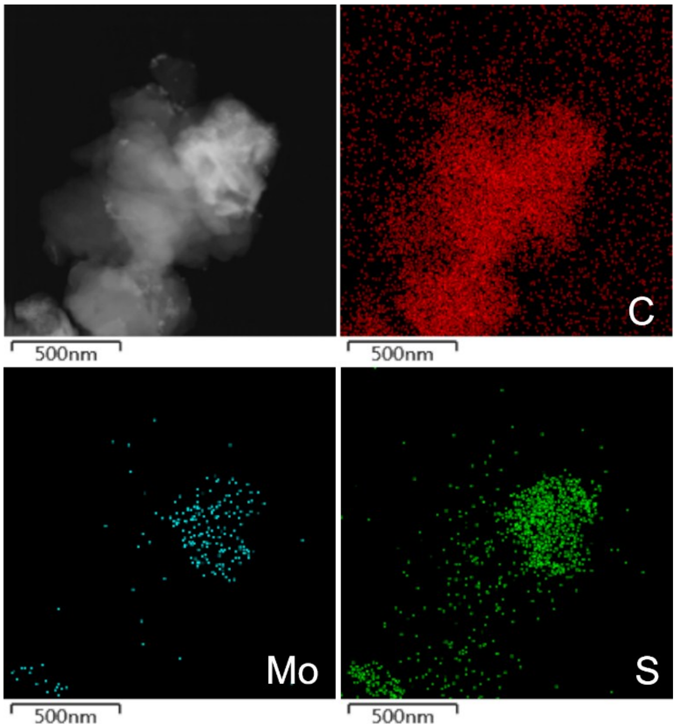

Figure S10. TEM image and the corresponding EDS elemental mapping images of C, Mo, S of the solid products from SZVR slurry-phase hydrocracking with MoS*x*-AN.

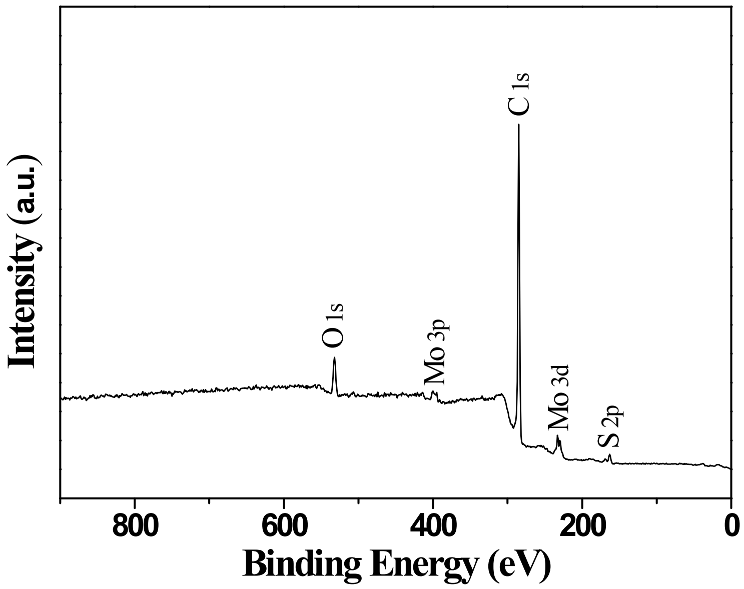

Figure S11. XPS survey spectra of the coke product from SZVR slurry-phase hydrocracking with MoS*x*-AM.

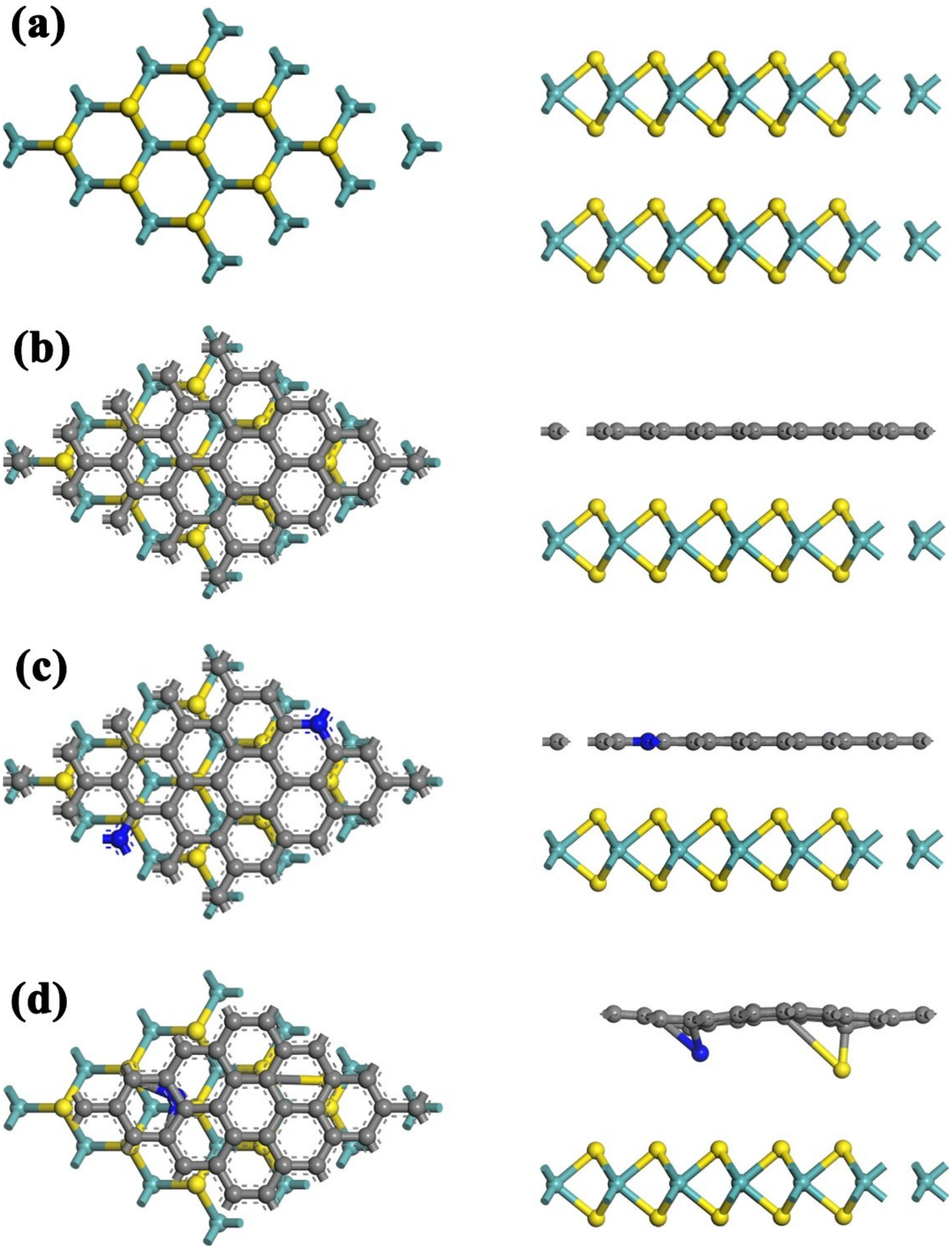

Figure S12. The incipient configurations of (a) MoS_2/MoS_2, (b) MoS_2/G, (c) MoS_2/N-G and (d) MoS_2/SN-G. Left are top views and right are front views. The C, S, N and Mo atoms shown are gray, yellow, blue and cyan spheres, respectively.

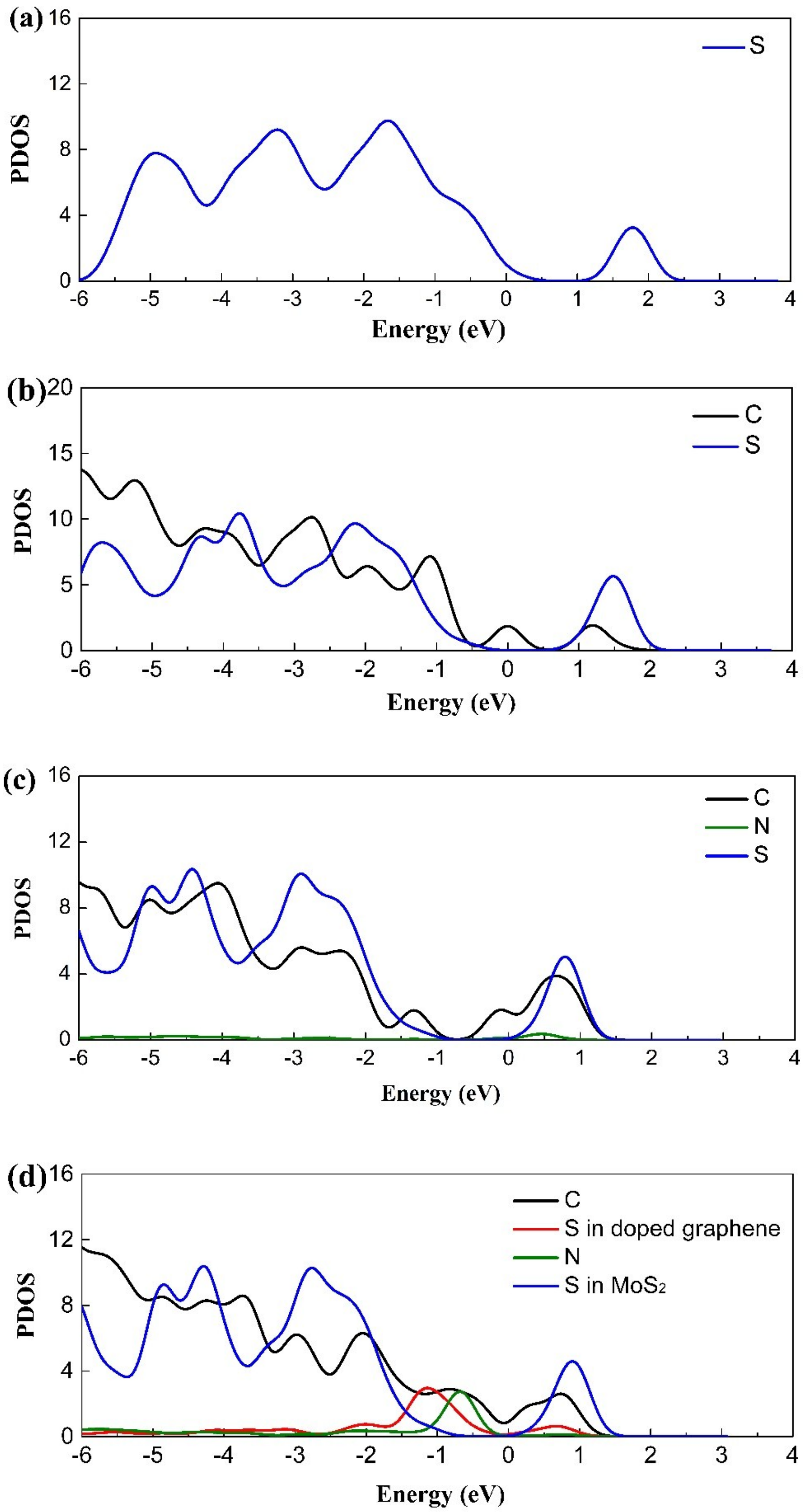

Figure S13. Partial density of states (PDOSs) of p orbitals of (a) MoS_2/MoS_2, (b) MoS_2/G, (c) MoS_2/N-G and (d) MoS_2/SN-G.